DOI: 10.1002/chem.200601475

Ionic Self-Assembly of Ammonium-Based Amphiphiles and Negatively Charged Bodipy and Porphyrin Luminophores

Franck Camerel,*[a] Gilles Ulrich,[a] Joaquín Barberá,[b] and Raymond Ziessel*[a]

Abstract: This paper describes the synthesis of wedge-shaped, charged amphiphilic molecules bearing an ammonium group at the tip that are able to organize negatively charged luminophores through an ionic self-assembly (ISA) process into discotic liquid-crystalline materials. For this purpose, two negatively charged luminescent molecules, 4,4-difluoro-1,3,5,7,8-pentamethyl-2,6-disulfonato-4-bora-3a,4a-diaza-*s*-indacene (sulfobodipy^{2-}) and tetrakis(4-sulfonatophenyl)porphyrin (TPPS^{4-}), were tested. The neutral luminescent complexes obtained through ISA form columnar mesophases that display hexagonal symmetry. Molecular modeling provides a structural description of the discotic mesophases in which the anionic luminophores are stacked in the middle of the disks. The key role of the amide linkage in the stabilization of the columnar architecture was probed by using infrared spectroscopy. Fluorescence microscopy has been used to show that the complexes are luminescent in both the solid and mesomorphic states.

Keywords: hydrogen bonds · liquid crystals · luminescence · porphyrinoids · self-assembly

Introduction

For almost two decades, interest in the use of luminescent molecules embedded in soft materials to create new electronic devices has gradually grown.[1] The design of luminescent and photoresponsive liquid crystals is particularly appealing owing to their potential applications in organic light-emitting diodes (OLED),[2] photovoltaic solar cells,[3] and organic field-effect transistors (OFET).[4] Amongst the various families of liquid-crystalline materials,[5] columnar mesophases engineered from disk-shaped molecules are particularly attractive owing to their unique charge transport properties, which include high mobility along the main axis of the column, and low intercolumn mobility owing to molecular segregation.[6] Additional advantages of columnar discotic liquid crystals over inorganic materials include their ease of processing (by using solution techniques), the possibility of alignment by means of shear forces or application of electrical or magnetic fields, and their capacity for self-healing.

In most cases, molecules that form discotic liquid crystals have a structure that consists of a flat central core with several carbon chains attached to the outside edge of the core. In some cases, discotic liquid-crystalline materials can also be formed by means of constructing a disk from two half-disk-shaped molecules.[7] The efficient use of discotic liquid-crystalline materials requires fine tuning of their mesogenic properties and phase symmetries, which are mainly controlled by the number of hydrocarbon chains and their positions. Typically, these materials have been produced by using conventional organic syntheses, which necessitates the complete development of a procedure for each structural variation.

Recently, a facile route to produce of highly organized supramolecular materials from a variety of charged building blocks, by means of complexation with surfactants, was introduced.[8] In general, ionic self-assembly (ISA) is a technique that organizes multiply charged organic species by means of their association with oppositely charged counterions, with the latter (e.g., surfactants) being functionalized

[a] Dr. F. Camerel, Dr. G. Ulrich, Dr. R. Ziessel
Laboratoire de Chimie Moléculaire
Ecole Chimie, Polymères, Matériaux (ECPM)
Université Louis Pasteur-CNRS (UMR 7509)
25 rue Becquerel, 67008 Strasbourg Cedex (France)
Fax: (+33) 390-242-635
E-mail: fcamerel@chimie.u-strasbg.fr
ziessel@chimie.u-strasbg.fr

[b] Dr. J. Barberá
Departamento de Química Orgánica
Instituto de Ciencia de Materiales de Aragón
Universidad de Zaragoza-CSIC, 50009 Zaragoza (Spain)

Supporting information for this article is available on the WWW under http://www.chemeurj.org/ or from the author. It contains a complete experimental section, which includes the preparation, thermal behavior, and X-ray characterization of the $C_n$amine. Color versions of Figures 2, and 4–7, are also included.

to have desirable properties. Hierarchical superstructures can then be generated in an ISA process, primarily through electrostatic interactions between charged surfactants and oppositely charged oligoelectrolytes. Hydrophobic and π–π interactions act as the secondary driving forces to promote self-organization. Additional interactions, such as hydrogen bonding, can also be introduced to further stabilize and control the organization of the assemblies.[9] The construction of liquid-crystalline materials based on stepwise noncovalent interactions allows the properties of the new structures to be easily tuned through the careful choice of the alkyl volume fraction ("internal solvent") by simply exchanging the cation in the assembly step without tedious synthetic operations. For example, introduction of double-tail surfactants, which enlarge the alkyl volume fraction within the materials, produces soft materials that display thermotropic liquid-crystalline materials from very rigid tectonic units.[10] Thus, ISA has been successfully used to organize various types of charged oligomeric species, such as dyes,[10a,11] dendrimers,[12] oligoanilines,[13] inorganic polymetallic molecules,[14] perylene derivatives,[15] and coordination complexes,[16] into well-ordered liquid-crystalline materials.

In most cases, standard, commercially available, charged surfactants have been used, however, more elaborate amphiphilic molecules that are able to introduce new functionalities, such as hydrogen bonding, chirality, or polymerizable groups inside the ionic self-assembled materials, remain elusive. A limited number of papers have described the use of functional synthetic surfactants in ISA processes.[17] Recently, wedge-shaped molecules with sulfonic acid groups at the focal point were found to display self-assembling capabilities to form mesomorphic materials or an extended network of fibers that form a gel in organic solvents.[18]

Liquid-crystalline porphyrins have received considerable attention as materials for molecular electronics owing to their ability to act as unidimensional conductors and semiconductors.[19] However, 4,4-difluoro-4-bora-3a,4a-diaza-*s*-indacene (*F*-bodipy) derivatives are known to exhibit remarkable optoelectronic properties, such as strong absorption in the visible region, high fluorescence quantum yields, and narrow emission bandwidths with high peak intensities, and rarely produce liquid-crystalline materials and supramolecular gels.[20]

In the present work, we wish to describe the synthesis of new, charged, wedge-shaped amphiphilic molecules with ammonium groups at the tip that are able to use ISA processes to organize negatively charged, luminescent dyes into columnar liquid-crystalline materials. These charged amphiphiles were specially designed to contain an amide linkage to direct, control, and stabilize the molecular architecture of oppositely charged functional molecules. The ability of these charged ammonium amphiphiles to organize anionic fluorophores into liquid-crystalline materials by using ionic interactions was tested with 4,4-difluoro-1,3,5,7,8-pentamethyl-2,6-disulfonato-4-bora-3a,4a-diaza-*s*-indacene (sulfobodipy^{2-}) and tetrakis(4-sulfonatophenyl)porphyrin (TPPS^{4-}).

Abstract in French: *Ce travail présente la synthèse de molécules amphiphiles portant un groupement ammonium polaire et une fonction amide structurante capable d'organiser des molécules luminescentes chargées négativement en mésophases thermotropes discotiques par auto-assemblage par voie électrostatique. Pour démontrer l'habilité de ces molécules ambipolaire à pouvoir s'organiser en phase cristal-liquide des molécules négativement chargées et luminescentes portants des groupements sulfonates, le bodipy disulfonate (sulfobodipy^{2-}) et la porphyrine tétrasulfonate (TPPS^{4-}), ont été facilement associées. Les complexes neutres et luminescents obtenus par auto-assemblage électrostatique forment des mésophases colonnaires de symétrie 2D hexagonale. Une modélisation moléculaire simplifiée permet de décrire ces phases cristal-liquide comme étant constituées de colonnes formées par des empilements de disques. Une micro-ségrégation entre les luminophores au centre et les molécules amphiphiles à la périphérie permet de décrire la formation de ces unités discoïdes. Le rôle de la liaison hydrogène dans la stabilisation de cette architecture colonnaire est confirmée par spectroscopie infrarouge. La microscopie par fluorescence montre d'autre part que ces composés mésomorphes sont luminescents à l'état solide.*

Abstract in Spanish: *Este artículo describe la síntesis de moléculas anfifílicas cargadas con forma de cuña y con un grupo amonio en la punta, que son capaces de organizar luminóforos cargados negativamente a través de un proceso de auto-ensamblaje iónico para generar materiales liquido-cristalinos discóticos. Con este objetivo, se han examinado dos moléculas luminiscentes cargadas negativamente, un disulfonato-tetrametilpirrometeno-BF_2 (sulfobodipy^{2-}) y una tetrasulfonato-tetrafenilporfirina (TPPS^{4-}). Los complejos luminiscentes neutros obtenidos por auto-ensamblaje iónico forman mesofases columnares con simetría hexagonal. La modelización molecular aporta una descripción estructural de las mesofases discóticas con los luminóforos aniónicos apilados en el centro de los discos. La espectroscopia infrarroja ha demostrado el papel decisivo del enlace amida en la estabilización de la arquitectura molecular. La microscopia de fluorescencia ha mostrado que los complejos son luminiscentes tanto en el estado sólido como en el mesomorfo.*

Results and Discussion

Synthesis: The preparation of the ammonium amphiphiles is outlined in Scheme 1. 3,4,5-Tri(*n*-alkyloxy)benzoic acid chlorides ($n=8$, 12, 14, 16)[21] were treated with *N*,*N*-dimethyl-1,4-phenylenediamine dihydrochloride in dry dichloromethane by using triethylamine as the base. The amido derivatives were isolated by means of chromatography on silica gel and subsequent methylation was achieved by heating the amido derivatives at reflux in neat iodomethane to give the ammonium iodine salts in quantitative yields. Note

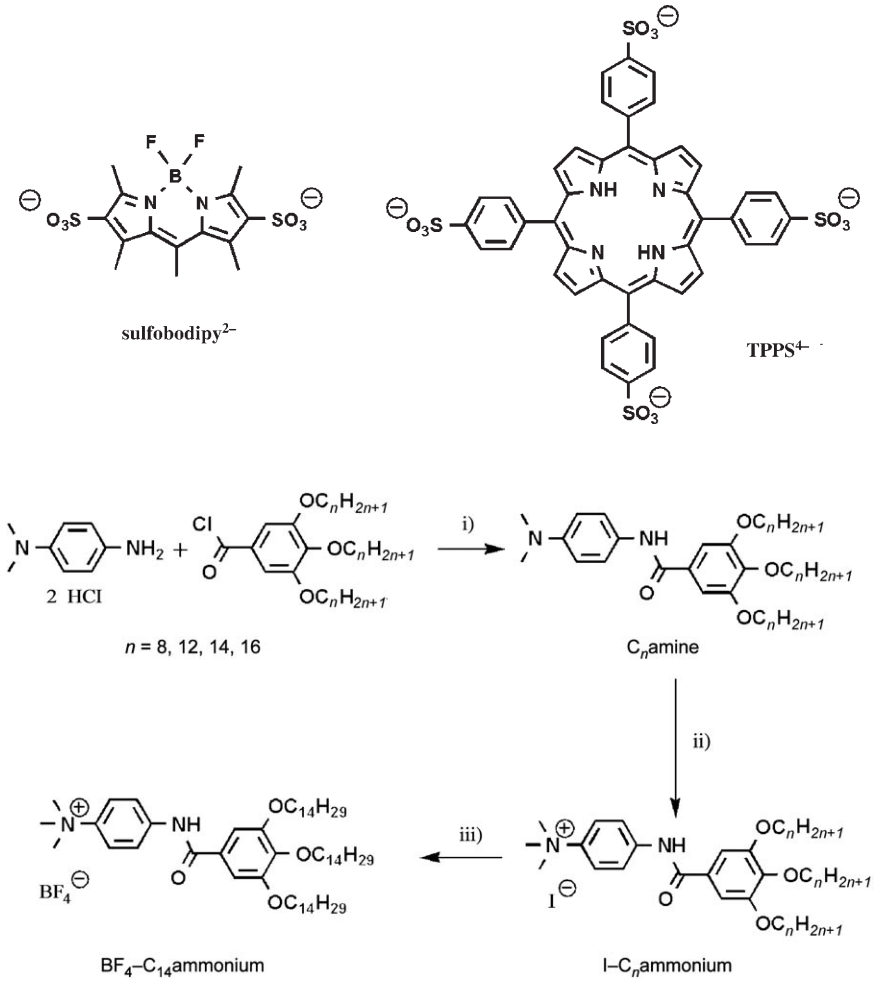

Scheme 1. Reagents and conditions: i) anhydrous CH_2Cl_2, NEt_3 (4 equiv), RT; $n=8$ (46%), $n=12$ (58%), $n=14$ (56%), $n=16$ (76%); ii) CH_3I, reflux (99%); iii) $AgBF_4$, ethanol.

that the NH group of the amide is not affected by using a large excess of CH_3I. Anion exchange from iodine to tetrafluoroborate was assured by treating the iodo salt with $AgBF_4$ in ethanol.

Complexes formed by means of ion association between sulfobodipy^{2-}[22] and TPPS^{4-} anions and the various ammonium cations were obtained from metathesis reactions, which resulted in their precipitation as their iodide or sodium salts when water was added to solutions of the anions in DMF. The resulting adducts (complexes) were recrystallized from a mixture of dichloromethane/acetonitrile. Complexation ratios of 2:1 for sulfobodipy^{2-} and 4:1 for TPPS^{4-} were confirmed by means of elemental analyses and NMR spectroscopy. The sulfobodipy^{2-} complexes were isolated with ammonium salts that contained C_{12}, C_{14}, and C_{16} paraffin chains, whereas the TPPS^{4-} complexes could only be readily isolated with ammonium salts that contained C_8 and C_{12} paraffin chains.

Optical properties in solution: Solutions of bodipy compounds in dichloromethane showed an intense $S_0 \rightarrow S_1$ (π–π^*) transition at around $\lambda=510$ nm with an extinction coefficient of $\varepsilon=25\,000$–$30\,000\,M^{-1}cm^{-1}$, which was unambiguously assigned as π–π^* transitions of the boradiazaindacene chromophore (Table 1). A weak, broad band located at $\lambda=375$ nm was attributed to the $S_0 \rightarrow S_2$ (π–π^*) transition of the boradiazaindacene core.[23] For the porphyrin derivatives, a strong Soret band was observed at $\lambda=418$ nm and characteristically weak Q bands were observed between $\lambda=515$ and 648 nm, with a Qx(0–0) band at 648 nm.[24] For all the solutions of bodipy complexes in dichloromethane, excitation in the band at $\lambda=510$ nm ($S_0 \rightarrow S_1$ transition) led to a strong emission in the $\lambda=538$–540 nm region with quantum yields in the range of 20 to 30%, which is typical for bodipy dyes. The fluorescence spectrum shows good mirror symmetry in which the lowest energy absorption transition and the quantum yield are not sensitive to the presence of oxygen. Both trends are consistent with the radiative relaxation of a singlet excited state. Furthermore, the fluorescence decay profiles can be described by means of a single exponential fit, with fluorescence lifetimes in the range of four to six nanoseconds, which is also in accordance with a singlet excited state. Excitation in the lowest-energy Q band of the porphyrin systems produces weak luminescence bands at $\lambda \approx 660$ and 721 nm ($\phi \approx 3\%$).

Thermal studies: The thermal behavior of $C_n$amine, $C_n$ammonium, and the ionic complexes was investigated by means of polarizing optical microscopy (POM) and differential scanning calorimetry (DSC). The transition temperatures and enthalpies are gathered in Table 2.

$C_n$amine: All the $C_n$amine compounds displayed a single reversible transition in the DSC curves that were unambiguously assigned by means of POM to the direct melting of the crystalline phase into the isotropic phase.

$C_n$ammonium: All the as-prepared $C_n$ammonium iodide salts appeared to be unstable above 120°C. However, exchanging the I^- counteranion for BF_4^- enhanced their stability, and, for example, the C_{14}ammonium compound was then stable up to 185°C. On heating to 172°C, it can be observed

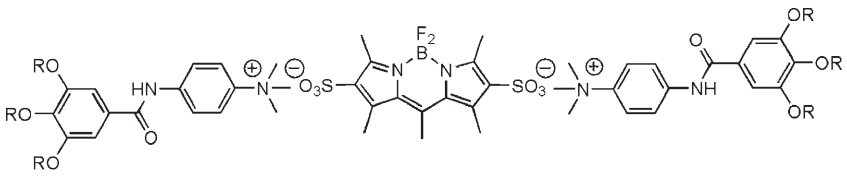

Sulfobodipy–$C_n$ammonium (n = 12, 14, 16)
R = $C_{12}H_{25}$, $C_{14}H_{29}$, $C_{16}H_{33}$

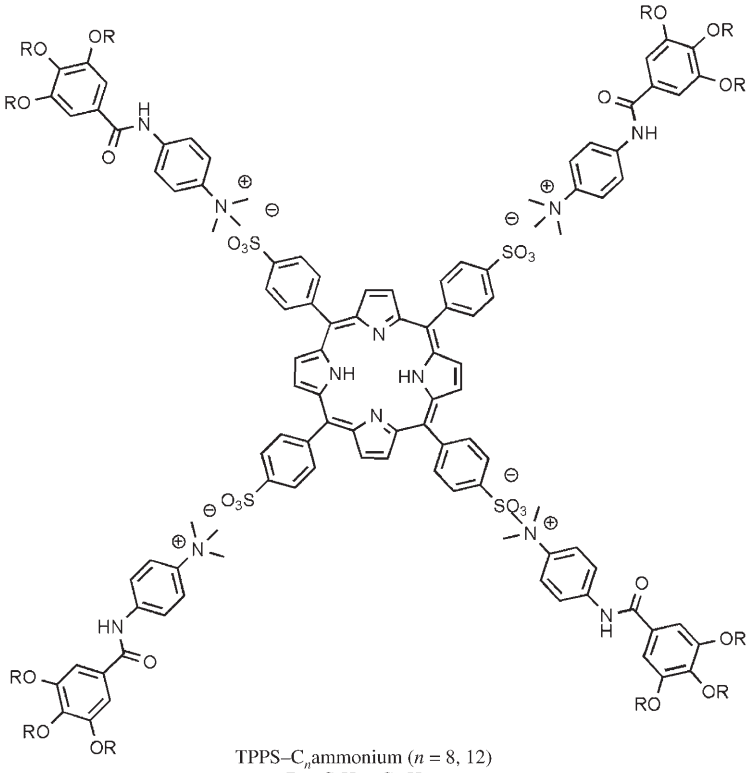

TPPS–$C_n$ammonium (n = 8, 12)
R = C_8H_{17}, $C_{12}H_{25}$

Table 1. Spectroscopic data for the various associated compounds.

Compounds	λ_{abs}[a] [nm]	ε[a] [$M^{-1}cm^{-1}$]	λ_F[a] [nm]	ϕ_F[b]	τ_F [ns]	k_r[c] [$10^7 s^{-1}$]	k_{nr}[c] [$10^8 s^{-1}$]
sulfobodipy–C_{12}ammonium	510	39500	540	20	4.9	4.08	1.63
sulfobodipy–C_{14}ammonium	509	35500	538	30	5.1	5.88	1.37
sulfobodipy–C_{16}ammonium	510	32500	539	25	5.1	4.90	1.47
TPPS–C_8ammonium	648	2450	658/721	4	–	–	–
	418	300000	658/721	3			
TPPS–C_{12}ammonium	648	3200	662/721	2	–	–	–
	418	360000	664/721	3			

[a] Measured in CH_2Cl_2 at RT. [b] Determined in dichloromethane (ca. 5×10^{-6} M) by using rhodamine 6G as a reference for bodipy compounds and cresyl violet as a reference for $TPPS^{4-}$. All ϕ_F are corrected for changes in refractive index. [c] Calculated by using $k_r=\phi_F/\tau_F$, $k_{nr}=(1-\phi_F)/\tau_F$, and assuming that the emitting state is produced with unit quantum efficiency.

that the compound melts into an isotropic state (Figure 1a). On cooling from the isotropic state, a characteristic texture develops between crossed-polarizers, and the concomitant observation of the soft nature of the material indicates the existence of a mesomorphic state (see below).

Sulfobodipy–$C_n$ammonium (n = 12, 14, 16): DSC measurements and NMR spectroscopic analyses revealed that these complexes are stable above 180 °C. Before heating, powders of all the compounds were birefringent between crossed-polarizers. The sulfobodipy–C_{12}ammonium complex does not show a transition on the DSC curves. POM observations showed that this compound was birefringent and a gel above 120–130 °C. The clearing point of this compound could not be precisely determined because degradation occurred above 180 °C, which prevented any clear textural assignment of the phase symmetry. The observation of birefringence in the gel at high temperatures confirmed its liquid-crystalline nature. After the first heating cycle, the sulfobodipy–C_{14}ammonium and sulfobodipy–C_{16}ammonium complexes displayed a broad, reversible transition that was centered at −2 and 11 °C, respectively (Figure 1b). This broad transition is typical for structural rearrangements of the aliphatic chains (melting of the carbon chains). Above 100 °C, these compounds also become highly viscous and birefringent, which are good indications of their mesomorphic nature (Figure 2a and b).

TPPS–$C_n$ammonium (n = 8, 12): DSC measurements and NMR spectroscopic analysis showed that degradation occurred at around 170 °C. For both complexes (C_8 and C_{12}), no transition was apparent on the DSC curves. Before heating, these compounds were slightly birefringent powders. An increase in temperature rendered these materials less viscous and more birefringent. The gel-like nature of these birefringent materials at high temperatures reflects their mesomorphic state (Figure 2c and d).

XRD characterization and mesomorphic behavior: Excluding the crystalline $C_n$amine compounds, BF_4–C_{14}ammonium and associated ISA complexes were subjected to a range of temperature-dependent wide/small-angle X-ray scattering (WAXS/SAXS) measurements to elucidate their morphologies.

Table 2. Thermal behavior and X-ray characterization of the liquid-crystalline phases.

Compound	T_{onset} [°C][a] (ΔH [kJ mol^{-1}])	d_{meas} [Å][b]	I[c]	hk[d]	d_{calcd} [Å][b]	mesophase parameters[e]	V_m [Å^3][f]	M_r [g mol^{-1}]
BF_4–C_{14}ammonium	Col_h 172 (0.9) Iso	41.1	vs	10	41.0	T=150 °C	1716	979
	Iso 160 (−1.1) Col_h	23.5	m	11	23.7	a=47.4 Å		
		20.6	w	20	20.5	S=1943 Å^2		
		4.65	br	A				
		42.0	vs	10	42.0	T=100 °C	1777	
		24.5	m	11	24.3	a=48.5 Å		
		20.8	w	20	21.0	S=2037 Å^2		
		4.5	br	A				
sulfobodipy–C_{12}ammonium	Col_h 180 (decomp)	45.7	vs	10	45.7	T=125 °C	3637	2038
		26.8	m	11	26.4	a=52.8 Å		
		22.5	w	20	22.9	S=2413 Å^2		
		4.5	br	A				
		44.0	vs	10	44.3	T=25 °C	3384	
		25.8	m	11	25.6	a=51.2 Å		
		22.1	w	20	22.2	S=2268 Å^2		
		4.4	br	A				
sulfobodipy–C_{14}ammonium	Cr −2 (10.4) Col_h 180 (decomp)	50.0	vs	10	49.5	T=100 °C	3870	2207
		28.7	m	11	28.6	a=57.2 Å		
		24.3	w	20	24.8	S=2831 Å^2		
		4.5	br	A				
		51.9	vs	10	51.8	T=25 °C	3665	
		30.1	m	11	29.9	a=59.8 Å		
		25.6	w	20	25.9	S=3098 Å^2		
		4.4	br	A				
sulfobodipy–C_{16}ammonium	Cr 11 (6.9) Col_h 180 (decomp)	51.7	vs	10	51.4	T=100 °C	4164	2375
		29.8	m	11	29.7	a=59.4 Å		
		25.4	w	20	25.7	S=3053 Å^2		
		4.5	br	A				
		50.7	vs	10	50.4	T=25 °C	3944	
		29.1	m	11	29.1	a=58.2 Å		
		25.0	w	20	25.2	S=2933 Å^2		
		4.4	br	A				
TPPS–C_8ammonium	Col_h 170 (decomp)	40.1	vs	10	40.1	T=140 °C	6293	3490
		20.0	m	20	20.05	a=46.3 Å		
		16.2	w	–	–	S=1857 Å^2		
		4.6	br	A				
		39.0	vs	10	39.0	T=25 °C	5795	
		19.5	m	20	19.5	a=45.0 Å		
		15.5	w	–	–	S=1755 Å^2		
		4.6	br	A				
TPPS–C_{12}ammonium	Col_h 170 (decomp)	47.7	vs	10	47.8	T=140 °C	7509	4164
		27.6	m	11	27.6	a=55.2 Å		
		24.0	w	20	23.9	S=2639 Å^2		
		4.5	br	A				
		47.4	vs	10	47.4	T=25 °C	6915	
		27.2	m	11	27.35	a=54.7 Å		
		23.8	w	20	23.7	S=2593 Å^2		
		4.4	br	A				

[a] Cr: crystalline phase, Iso: Isotropic liquid, Col_h: hexagonal columnar mesophase, decomp: decomposition temperature (evaluated from the deviation of the baseline on the DSC and confirmed by means of POM observations) [b] d_{meas} and d_{calcd} are the measured and calculated diffraction peak spacings, respectively. [c] I is the intensity of the reflection; vs: very strong, m: medium, w: weak, br: broad. [d] The indexation of the reflections corresponding to Col_h phase. [e] Measured at temperature T, a is the lattice parameter of Col_h ($a=\frac{2}{\sqrt{3}}\times<d_{10}>$, in which $<d_{10}>=\frac{1}{N_{hk}}(\sum_{h,k} d_{hk}\sqrt{h^2+k^2+hk})$ and N_{hk} is the number of hk reflections); S is the lattice area ($S=a\times<d_{10}>$ for Col_h). [f] The molecular volume V_m was measured at temperature T and is defined by $V_m=(M_r/0.6022)/(V_{CH_2}(T)/V_{CH_2}(T_0))$ in which $V_{CH_2}(T)=26.5616+0.02023T$ (T in °C, T_0=25 °C).

BF_4–C_{14}ammonium: The XRD pattern recorded at 100 °C was characteristic of a hexagonal columnar (Col_h) mesophase (Figure 3a). It contained a set of three sharp maxima in the low-angle region: a strong reflection at 42.0 Å and two weaker reflections at 24.5 and 20.8 Å. These spacings were in the reciprocal ratio of 1:$\sqrt{3}$:2, and could be indexed as the (10), (11), and (20) reflections of a two-dimensional hexagonal lattice, respectively, with a lattice constant of a= 48.5 Å. Aside from this, a characteristically diffuse halo was found at around 4.5 Å. The same kind of XRD pattern, characteristic of a Col_h mesophase, was obtained at 150 °C. However, the three low-angle maxima were shifted to higher angles and the diffuse halo became broader and shifted to lower angles. Thus, the hexagonal lattice constant at

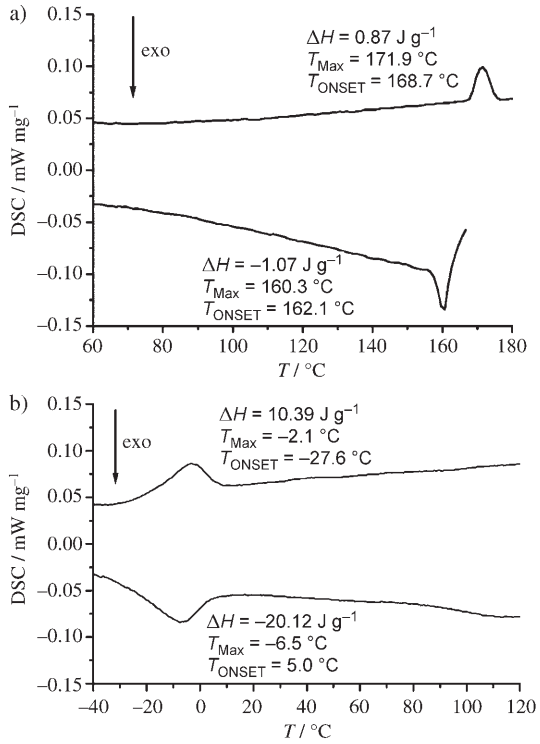

Figure 1. DSC traces of a) BF_4–C_{14}ammonium and b) sulfobodipy–C_{14}ammonium. In each case, the top curve shows the second heating curve and the bottom curve shows the first cooling curve.

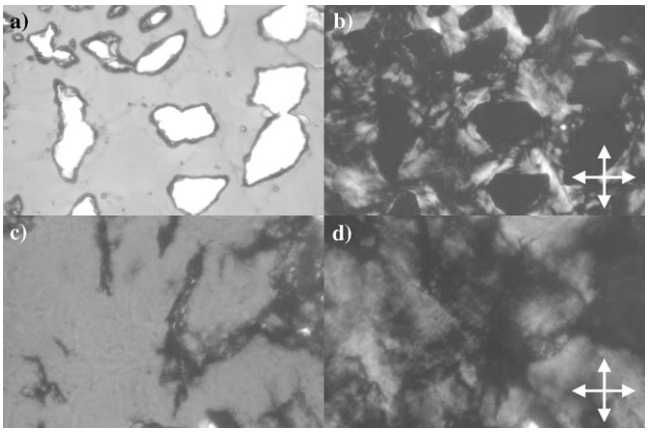

Figure 2. a) Gel state of sulfobodipy–C_{16}ammonium observed by using optical microscopy without polarizers at 150 °C. b) Same birefringent area observed by using optical microscopy between crossed-polarizers (indicated by the cross in the corner of the picture). c) TPPS–C_{12}ammonium in its gel state at 150 °C. d) Same birefringent area observed between crossed-polarizers.

this temperature decreased to $a = 47.4$ Å and the average lateral distance increased to about 4.65 Å. The variations in distance with temperature are consistent with the higher conformational disorder of the hydrocarbon chains, which occurs as the temperature increases.

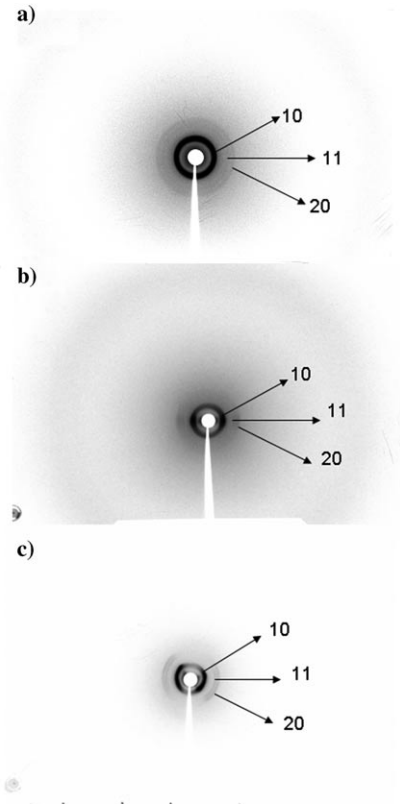

Figure 3. XRD patterns of a) BF_4–C_{14}ammonium in the hexagonal columnar mesophase at 100 °C, b) sulfobodipy–C_{12}ammonium in the hexagonal columnar phase at room temperature after heating at 125 °C, and c) TPPS–C_{12}ammonium in the hexagonal columnar phase at room temperature after heating at 161 °C.

It seems likely that the columns are generated through anion stacking, in which the cations are attached perpendicularly to the column axis so that their charged heads lie close to that axis and the aliphatic chains lie on the periphery (see below).

Sulfobodipy–$C_n$ammonium (n = *12, 14, 16):* The XRD patterns of sulfobodipy–C_{12}ammonium, recorded at 125 °C and at room temperature (after heating at 150 °C), were typical for a hexagonal columnar (Col_h) mesophase. The low-angle region contained a set of three sharp maxima with scattering vectors in the ratio of $1:\sqrt{3}:2$ and were indexed as the (10), (11), and (20) reflections of a two-dimensional hexagonal lattice. From the spacing of these reflections, it was deduced that the hexagonal lattice constant was $a = 52.8$ Å at 125 °C (Figure 3b). Aside from the low-angle reflections mentioned previously, no other Bragg spots were detected by using X-rays. A diffuse, wide halo was observed in the high-angle region at 4.4 to 4.5 Å and is characteristic of the conformational disorder of the hydrocarbon chains. A similar pattern was obtained at 25 °C and confirmed that sulfobodipy–C_{12}ammonium is a columnar liquid crystal with hexagonal symmetry at room temperature. The X-ray results for the C_{14}ammonium complex are similar to those obtained for the C_{12}ammonium complex. Its XRD patterns displayed a set of

three sharp maxima with scattering vectors in the ratio of $1:\sqrt{3}:2$, but were shifted to lower angles, which implied that the compound has a larger hexagonal lattice constant ($a=57.2$ Å) at 100 °C. The diffuse, wide halo observed at 4.4 to 4.5 Å in the high-angle region also confirmed the liquid-crystalline nature of this compound both at room and high temperatures. The XRD patterns recorded for sulfobodipy–C_{16}ammonium were also typical of a columnar hexagonal phase (Col_h) and the deduced hexagonal lattice constant at high temperature was $a=59.4$ Å. The increase in the lattice constant observed when going from the C_{12} to the C_{16} complexes appeared to be consistent with the increase in the chain length. The XRD results obtained confirm that all of the sulfobodipy–$C_n$ammonium complexes studied are mesomorphic with (Col_h) mesophases from room temperature up to 150 °C.

TPPS–$C_n$ammonium (n = *8, 12)*: The X-ray pattern recorded on a TPPS–C_{12}ammonium sample cooled from 161 °C to room temperature was typical of a Col_h mesophase. The low-angle region contained a set of three sharp maxima with reciprocal spacings in the ratio of $1:\sqrt{3}:2$ and a hexagonal lattice constant ($a=54.7$ Å) could be deduced from this set of reflections (Figure 3c). A broad halo was also observed at 4.4 Å in the wide-angle region and confirmed the fluidlike nature of this phase at room temperature. For the TPPS–C_8ammonium complex, the X-ray patterns recorded at 140 °C and on a sample cooled from 163 °C to room temperature were very similar. The low-angle region contained a set of two sharp maxima with scattering vectors in the ratio of 1:2, with *d*-spacing values of 39 and 19.5 Å, respectively. This ratio has two possible interpretations: 1) the two peaks are the first- and second-order reflections, respectively, from a layered structure (smectic mesophase). The spacing of the first reflection is the layer thickness; 2) the two peaks are the (10) and (20) reflections from a Col_h mesophase, respectively, and the (11) reflection is absent. The mesophase was assigned as a Col_h phase after considering the results obtained with TPPS–C_{12}ammonium, the molecular shape, and the mesomorphic behavior of structural analogues.[26] This interpretation was also supported by comparing the measured spacings with the molecular dimensions estimated by using Dreiding stereomodels. Thus, the diffraction peak observed at lower angles in the X-ray pattern would correspond to the fundamental reflection of a hexagonal lattice with a lattice parameter of $a=45.0$ Å at room temperature.

Infrared spectra of the mesophases: The role of the amide functionality in intermolecular hydrogen bonding within the different architectures encountered was studied by using FTIR spectroscopy, which is a powerful tool to probe hydrogen bonding and hydrocarbon chain ordering in various states of matter. The frequencies of the bands that correspond to CH_2 antisymmetric and symmetric modes ($\nu_a(CH_2)$ and $\nu_s(CH_2)$) of the alkyl chains appear in the ranges $\tilde{\nu}=2916$ to 2924 and 2848 to 2854 cm^{-1}, respectively, for all the compounds in crystalline or mesophase states and correspond to some ordering of the hydrocarbon chains with an all-*trans* conformation.[27] Band shifts to higher frequencies occur as the chain packing tends to become more disordered.

At room temperature in the crystalline state, all the amide groups of the $C_n$amine compounds are involved in forming strong hydrogen bonds, as clearly indicated by the ν_{NH} and ν_{CO} stretching vibrations that lie in the ranges of $\tilde{\nu}=3206$ to 3247 and 1633 to 1636 cm^{-1}, respectively.[28,29] Note that values for free amides usually lie between $\tilde{\nu}=3500$ and 3400 cm^{-1} for ν_{NH} and at around 1680 cm^{-1} for ν_{CO}.[29] The presence of single ν_{NH} and ν_{CO} stretching bands in the IR spectra suggests the formation of a well-organized hydrogen-bonded network in which only one type of hydrogen bond is effective.

For BF_4–C_{14}ammonium, the FTIR spectra obtained before and after heating at 110 °C were almost identical, with one ν_{CO} stretching vibration centered at $\tilde{\nu}=1656$ cm^{-1} and one ν_{NH} stretching vibration centered at $\tilde{\nu}=3343$ cm^{-1}, which are clear signatures of amide functions engaged in hydrogen bonds.

For sulfobodipy–$C_n$ammonium complexes in which $n=12$, 14, or 16 and TPPS–$C_n$ammonium complexes in which $n=8$ or 12, the FTIR spectra obtained are essentially identical to that of the BF_4–C_{14}ammonium compound. The as-prepared complexes display a single broad ν_{CO} stretching vibration centered at $\tilde{\nu}=(1654\pm4)$ cm^{-1} and two ν_{NH} stretching vibrations centered at $\tilde{\nu}=(3294\pm20)$ and (3403 ± 6) cm^{-1} with equal intensities. The FTIR spectra are characteristic for materials in which some of the NH groups are not involved in hydrogen bonds. After the samples have been heated, the FTIR spectra measured at room temperature display one ν_{CO} stretching vibration centered at $\tilde{\nu}=(1644\pm6)$ cm^{-1} and one ν_{NH} stretching vibration centered at (3304 ± 4) cm^{-1}, which indicate the formation of a hydrogen-bonded network that involves all of the amide functions. Finally, the S–O stretching vibration and deformation bands of the sulfonate groups found at around $\tilde{\nu}=1190$ and 1117 cm^{-1} for the sulfobodipy–ammonium complexes and at around $\tilde{\nu}=1200$ and 1114 cm^{-1} for the TPPS–ammonium complexes differ significantly from those of the starting (Na_2–sulfobodipy) ($\tilde{\nu}_{SO}=1180$ and 1094 cm^{-1}) and (Na_4–TPPS) ($\tilde{\nu}_{SO}=1183$ and 1119 cm^{-1}) salts.

Packing study of the ISA complexes: To gain some insight into the packing of the ISA complexes inside the columnar liquid-crystalline phases, a standard geometric treatment was applied.[30] Columnar packing is characterized by using two structural parameters,[31] the columnar cross-section S_{col}, and the stacking periodicity h along the columnar axis. Both parameters are analytically linked through the relationship shown in Equation (1):

$$hS_{col} = ZV_m \quad (1)$$

in which Z is the number of molecules within a columnar stratum (disk) and V_m is the molecular volume. On XRD

patterns, neither peaks nor halos, related to the stacking periodicity h, have been observed. In this situation, it is difficult to determine the number of molecules per disk and only rough estimations can be made. From the previous analytical relationship, the thickness of the disk can be estimated by considering the number of molecules per disk (Z) as a variable, as shown in Equation (2):

$$h = \frac{Z \times V_m}{a \times d_{10}} \quad (2)$$

For example, for the BF_4–C_{14}ammonium complex at 100 °C, there must be between four and five molecules per disk (for $Z=4$, $h=3.4$ Å; for $Z=5$, $h=4.2$ Å). At 150 °C, the estimates obtained for $Z=4$ and 5 were, $h=3.7$ and 4.6 Å, respectively. This implies that each disk, which generates columns through stacking, is generated by several molecules (Figure 4). The ionic groups are located in the center

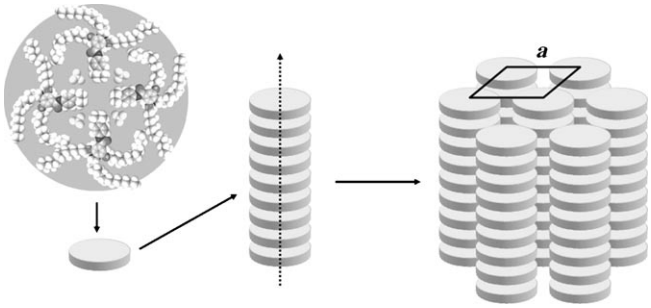

Figure 4. Suggested molecular organization inside the hexagonal columnar phase based on X-ray data obtained for BF_4–C_{14}ammonium.

of the disk and the peripheral chains surround the central ionic region. In this way, an optimal microsegregation between the aliphatic parts and the polar parts inside a disk is guaranteed. The hydrocarbon chains are able to efficiently fill the peripheral space around the columnar core. The mutual organization of these columns into a hexagonal lattice leads to the formation of the mesophase.

For sulfobodipy–$C_n$ammonium complexes, the same type of calculation leads to the conclusion that there must be about three to four molecules per disk at room temperature (sulfobodipy–C_{12}ammonium: $h=3.0$ Å for $Z=2$ (too small) and $h=4.5$ Å for $Z=3$; sulfobodipy–C_{14}ammonium: $h=3.6$ Å for $Z=3$ and $h=4.7$ Å for $Z=4$; sulfobodipy–C_{16}ammonium: $h=4.0$ Å for $Z=3$ and $h=5.4$ Å for $Z=4$). In regards to their overall shape, which can be compared to a large rod that has an electrostatically assembled core and three chains at each end, sulfobodipy^{2-} compounds behave as phasmidic liquid crystals.[5b] The molecules generate clusters of about three to four molecules that are able to stack in columns (Figure 5).[32] However, this is a simplified model because the molecules can in fact aggregate in such a way that the cations are randomly oriented, and just their tips point towards the stacked anion column that is built up from sheets of more than one anion without the need to

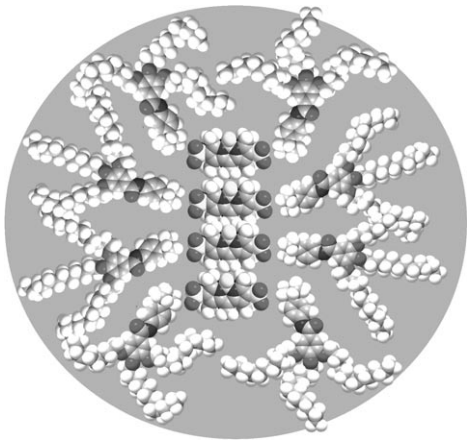

Figure 5. Suggested molecular organization inside a single disk based on X-ray data obtained for sulfobodipy–C_{12}ammonium.

form discrete disks. Because of its particular shape, each molecule is able to fill a portion of the column cross-section without necessarily lying coplanar with the anion sheet and it is these columns that assemble to form a two-dimensional hexagonal lattice.[33]

TPPS derivatives are known to form extended one-dimensional rodlike structures in solution and in solid states through the formation of J-type aggregates (face-to-face stacking).[34] A typical stacking distance between porphyrin fragments of $\approx$3.5 Å is usually observed. This distance is also typical in liquid-crystalline porphyrin phases.[35] Taking this value as the stacking periodicity h, a value of $Z=1$ is determined for the TPPS–$C_n$ammonium complexes. This value indicates that each disk forming the column is composed of one TPPS^{4-} molecule with its four surrounding ammonium counterions. Rotation of a molecule with respect to the adjacent one inside the column may give rise to better space filling and organization of the pendant phenyl fragments carrying the sulfonate functions. It is likely that a mutual rotation of 45° occurs between two consecutive molecules to optimize molecular packing within the mesophase (Figure 6). This process allows a better arrangement of the chains around the central core of the columns, and thus, prevents the steric mismatch that could otherwise occur between the preferred core–core (3.5 Å) and chain–chain (4.5 Å) distances.

Solid-state luminescence: The luminescence properties of the ISA complexes were evaluated in the solid and mesophases states by using a fluorescence microscope equipped with a heating stage. All the compounds appear highly luminescent in the solid state when observed under UV light ($300<\lambda_{ex}<350$ nm; Figure 7). Solid-state measurements on sulfobodipy–$C_n$ammonium at room temperature, in a quartz capillary, revealed overlapping multiple emissions in the $\lambda=$ 520 to 650 nm range. Several solid-state aggregates are probably responsible for these broad emission envelopes (Figure 8). At room temperature, after heating at 150 °C, no significant changes to the emission spectra of the sulfobodi-

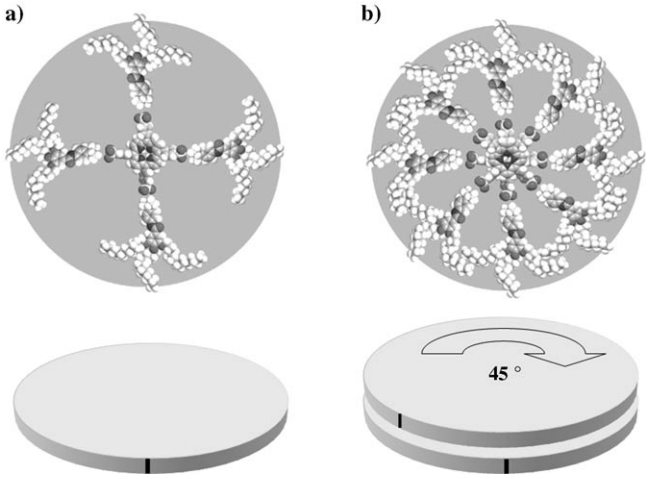

Figure 6. Organization of the TPPS–C_{12}ammonium complex inside a) a disk and b) along the column.

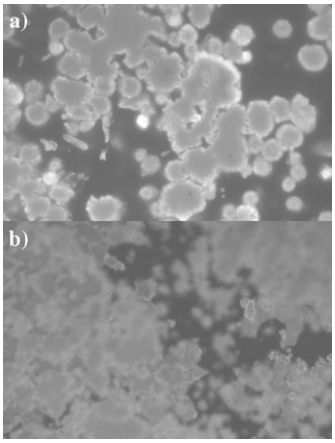

Figure 7. Solid-state emission observed for a) sulfobodipy–C_{16}ammonium and b) TPPS–C_{12}ammonium upon excitation at $300<\lambda_{ex}<350$ at room temperature.

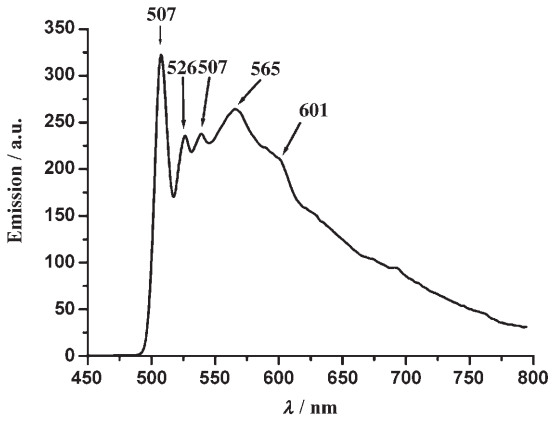

Figure 8. Solid-state emission spectrum of sulfobodipy–C_{16}ammonium ($\lambda_{ex}=370$ nm).

py–C_{16}ammonium, in the liquid-crystalline phase, were observed. This observation also supports the formation of aggregated species, even in the liquid-crystalline phase, and is in agreement with the proposed packing model of three to four molecules close-packed within a disk.

Upon heating, the materials become liquid-crystalline, which enables thin films to be formed readily. An unusual birefringent texture was observed by using POM (Figure 9a). The luminescence observed upon irradiation at

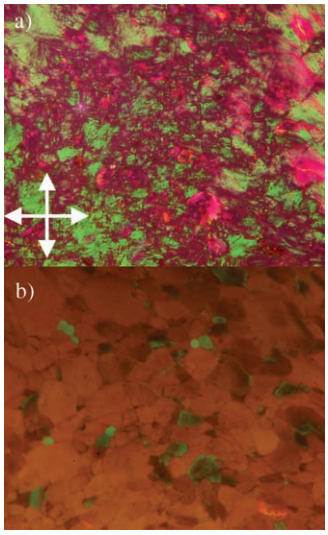

Figure 9. Textures of sulfobodipy–C_{16}ammonium observed by using optical microscopy at 150 °C with a) white light transmitted between crossed-polarizers (classical texture) and b) upon irradiation at $300<\lambda_{ex}<350$ nm without the polarizer.

$300<\lambda_{ex}<350$ nm without using a polarizer is not uniform and domains with different "real" color emissions can be observed (Figure 9b). The domains that emit green light appear redder by using POM, whereas the domains that emit pale orange light appear deep green between crossed polarizers. Thus, the emissions can be correlated to different molecular orientations inside the mesophase. It is noteworthy that the luminescence remains, even at elevated temperatures. The color modulation of the emitted light is correlated to the orientation of the domains, and therefore, to the column extension and orientation. These ISA complexes can be used as luminescent layers or thin films in which the homogeneity and the quality of the luminescent thin films can be easily checked by using fluorescence microscopy.

Conclusion

Our results show that the use of a central negatively charged sulfobodipy^{2-} or TPPS^{4-} template can provide mesomorphic materials through an ionic self-assembly process. Ammonium salts of amido derivatives of 3,4,5-trialkyloxybenzoic acid allow carbon chains of various lengths to be used without resynthesizing the key fluorescent molecule, which is

necessary for covalent architectures.[7c,d,20,21] The use of highly luminescent platforms allows the observation of the mesophase texture by means of fluorescence microscopy without using crossed-polarizers. In all cases, columnar mesophases with hexagonal symmetry were clearly identified by means of X-ray scattering measurements at various temperatures. From these data, it is estimated that for sulfobodipy–$C_n$ammonium complexes, three to four associated pairs form disks that then stack to form the column. Likewise, for the TPPS–$C_n$ammonium complexes, a single associated tetramer (one porphyrin and four surrounding ammonium derivatives) forms a disk. As confirmed by using infrared studies, the amido subunit in the ammonium framework is engaged in a supramolecular hydrogen-bonded network that stabilizes the thermotropic mesophases. Ionic self-assembled complexes provide a relatively easy way to produce liquid-crystalline materials and thin films that are stable over a large temperature range (RT to 180 °C), and are possibly useful for applications in energy-conversion devices. The flexibility resulting from the easy exchange of ionic components means that this method offers many additional possibilities to produce various soft materials, which incorporate more sophisticated scaffolding with particular optical, magnetic, and electronic properties. Work along these lines is currently in progress.

Experimental Section

General: The ^{1}H (300.1 MHz) and ^{13}C NMR (75.5 MHz) spectra were recorded at room temperature by using perdeuterated solvents as internal standards and are reported relative to the residual solvent. Mass spectrometry data were collected by using a ZAB-HF-VB instrument in FAB$^+$ mode with *m*-nitrobenzyl alcohol as the matrix. Chromatographic purification was conducted by using 40–63 μm silica gel. Thin-layer chromatography was performed on silica gel plates coated with fluorescent indicator. FTIR spectra were recorded by using a Perkin–Elmer Spectrum One spectrometer as thin films deposited onto dry KBr pellets. UV-visible spectra were recorded by using a UVIKON 940/941 dual-beam grating spectrophotometer (Kontron Instruments) with a 1 cm quartz cell. Fluorescence spectra were recorded by using a Perkin–Elmer LS50B spectrofluorimeter. All fluorescence spectra were corrected. The fluorescence quantum yield (ϕ_{expll}) was calculated from Equation (3):

$$\phi_{expl} = \phi_{ref} = \frac{F\{1-\exp(-A_{ref}\ln 10)\}n^2}{F_{ref}\{1-\exp(-A\ln 10)\}n_{ref}^2} \quad (3)$$

in which F denotes the integral of the corrected fluorescence spectrum, A is the absorbance at the excitation wavelength, and n is the refractive index of the medium. Rhodamine 6G ($\phi_{ref}=0.78$, $\lambda_{ex}=488$ nm) and cresyl violet ($\phi_{ref}=0.51$, $\lambda_{ex}=578$ nm)[25] were used as reference systems in air-equilibrated water.

Luminescence lifetimes were measured by using a PTI QuantaMaster spectrofluorimeter with TimeMaster software in Time-Correlated Single-Photon Mode coupled to a Stroboscopic system. The excitation source was a thyratron-gated flash lamp filled with nitrogen gas. No filter was used for the excitation. An interference filter centered at $\lambda=550$ nm selected the emission wavelengths. The instrument response function was determined by using a light-scattering solution (LUDOX). Differential scanning calorimetry (DSC) was performed by using a Netzsch DSC 200 PC/1/M/H Phox instrument equipped with an intracooler, which allowed measurements from −65 up to 450 °C to be recorded. The samples were examined at a scanning rate of 10 K min^{-1} by applying two heating and one cooling cycles. The apparatus was calibrated with indium (156.6 °C). Phase behavior was studied by means of POM by using a Leica DMLB microscope or a Leica DMLB fluorescence microscope equipped with a continuous 100 W mercury lamp, a Linkam LTS350 hot stage, and a Linkam TMS94 central processor. The XRD patterns were obtained with a pinhole camera (Anton-Paar) operating with a point-focused Ni-filtered $Cu_{K\alpha}$ beam. The samples were held in Lindemann glass capillaries (0.9 mm diameter) and heated, when necessary, with a variable-temperature oven. The patterns were collected on flat photographic film perpendicular to the X-ray beam. Spacings were obtained by using Bragg's law.

Materials: 3,4,5-Trialkyloxybenzoic acid chloride ($n=8$, 12, 14, 16) and 4,4-difluoro-1,3,5,7,8-pentamethyl-2,6-disulfonato-4-bora-3a,4a-diaza-*s*-indacene (sulfobodipy^{2-}) were synthesized as previously described. *N*,*N*-Dimethyl-1,4-phenylenediamine dihydrochloride (99 %) and tetrakis(4-sulfonatophenyl)porphyrin (Na_4–TPPS) were purchased from Aldrich and used as received.

General procedure for the preparation of ammonium compounds: $C_n$amine was heated at 60 °C in CH_3I, under argon overnight. The reactant/solvent was removed under vacuum, and recrystallization in dichloromethane afforded the desired $C_n$ammonium compound.

I–C_8ammonium: Reagents: C_8amine (1 g, 1.6 mmol), CH_3I (20 mL); yield: 89 % (1.1 g); ^{1}H NMR ($CDCl_3$, 300 MHz): $\delta=9.30$ (s, 1H), 7.88 (AB, $J_{A,B}=9.4$ Hz, $\nu_0=55.9$ Hz, 4H), 7.28 (s, 2H), 4.08 (t, $^3J=6.3$ Hz, 4H), 3.98 (t, $^3J=6.7$ Hz, 4H), 3.85 (s, 9H), 1.78–1.72 (m, 6H), 1.42–1.25 (m, 30H), 0.87–0.83 ppm (m, 9H); ^{13}C NMR ($CDCl_3$, 75 MHz): $\delta=166.3$, 153.0, 141.8, 141.5, 140.5, 128.3, 122.3 (CH), 120.3 (CH), 106.5 (CH), 73.5 (CH_2), 69.6 (CH_2), 57.9 (CH_3), 31.9 (CH_2), 31.8 (CH_2), 30.3 (CH_2), 29.5 (CH_2), 29.4 (CH_2), 29.3 (CH_2), 26.2 (CH_2), 26.1 (CH_2), 22.6 (CH_2), 14.1 ppm (CH_3); IR (KBr): $\tilde{\nu}=3426$ (br m), 3293 (br m), 2923 (s), 2854 (m), 1656 (m), 1582 (m), 1496 (s), 1334 (s), 1113 cm^{-1} (s); FABMS: *m*/*z* (%): 639.3 (100) $[M-I]^+$; elemental analysis calcd (%) for $C_{40}H_{67}IN_2O_4$: C 62.65, H 8.81, N 3.65; found: C 62.42, H 8.41, N 3.27.

I–C_{12}ammonium: Reagents: C_{12}amine (0.43 g, 0.54 mmol), CH_3I (10 mL); yield: 99 % (0.5 g); ^{1}H NMR ($CDCl_3$, 400 MHz): $\delta=9.40$ (s, 1H), 7.88 (AB, $J_{A,B}=9.2$ Hz, $\nu_0=79.5$ Hz, 4H), 7.29 (s, 2H), 4.09 (t, $^3J=6.3$ Hz, 6H), 3.96 (t, $^3J=6.4$ Hz, 3H), 3.84 (s, 9H), 1.81–1.74 (m, 6H), 1.25 (br s, 54H), 0.87 ppm (t, $^3J=6.2$ Hz, 9H); ^{13}C NMR ($CDCl_3$, 100 MHz): $\delta=$ 166.7, 153.5, 142.1, 141.9, 140.9, 128.7, 122.6 (CH), 120.7 (CH), 106.9 (CH), 73.9 (CH_2), 70.0 (CH_2), 58.4 (CH_3), 32.3 (CH_2), 30.8 (CH_2), 30.2 (CH_2), 30.15 (CH_2), 30.1 (CH_2), 30.05 (CH_2), 30.0 (CH_2), 29.9 (CH_2), 29.8 (CH_2), 26.7 (CH_2), 26.5 (CH_2), 23.1 (CH_2), 14.5 ppm (CH_3); IR (KBr): $\tilde{\nu}=3442$ (br m), 3293 (m), 2919 (s), 2850 (m), 1650 (s), 1582 (s), 1467 (s), 1424 (s), 1339 (m), 1121 cm^{-1} (s); FABMS: *m*/*z* (%): 808.2 (100) $[M-I]^+$; elemental analysis calcd (%) for $C_{52}H_{91}IN_2O_4$: C 66.78, H 9.81, N 3.00; found: C 66.49, H 9.62, N 2.64.

I–C_{14}ammonium: Reagents: C_{14}amine (0.84 g, 0.95 mmol), CH_3I (10 mL); yield: 74 % (0.71 g); ^{1}H NMR ($CDCl_3$, 300 MHz): $\delta=9.38$ (s, 1H), 7.85 (AB, $J_{A,B}=8.7$ Hz, $\nu_0=34.7$ Hz, 4H), 7.28 (s, 2H), 4.10–3.90 (m, 6H), 3.83 (s, 9H), 1.81–1.72 (m, 6H), 1.23 (br s, 66H), 0.85 ppm (m, 9H); ^{13}C NMR ($CDCl_3$, 75 MHz): $\delta=166.2$, 153.1, 141.5, 128.4, 122.1 (CH), 120.2 (CH), 106.5 (CH), 73.5 (CH_2), 69.5 (CH_2), 57.9 (CH_3), 31.9 (CH_2), 30.4 (CH_2), 29.8 (CH_2), 29.7 (CH_2), 29.6 (CH_2), 29.55 (CH_2), 29.5 (CH_2), 29.4 (CH_2), 26.2 (CH_2), 26.1 (CH_2), 22.7 (CH_2), 14.1 ppm (CH_3); IR (KBr): $\tilde{\nu}=3412$ (br w), 3293 (br m), 2918 (s), 2849 (s), 1648 (s), 1580 (m), 1533 (s), 1468 (s), 1424 (m), 1342 (m), 1122 cm^{-1} (s); FABMS: *m*/*z* (%): 892.0 (100) $[M-I]^+$; elemental analysis calcd (%) for $C_{58}H_{103}IN_2O_4$: C 68.34, H 10.18, N 2.75; found: C 67.84, H 9.82, N 2.43.

I–C_{16}ammonium: Reagents: C_{16}amine (0.81 g, 0.84 mmol), CH_3I (10 mL); yield: 92 % (0.86 g); ^{1}H NMR ($CDCl_3$, 300 MHz): $\delta=9.15$ (s, 1H), 7.85 (AB, $J_{A,B}=9.3$ Hz, $\nu_0=57.7$ Hz, 4H), 7.27 (s, 2H), 4.09 (t, $^3J=6.3$ Hz, 4H), 3.99 (t, $^3J=6.6$ Hz, 2H), 3.88 (s, 9H), 1.80–1.75 (m, 6H), 1.24 (br s, H), 0.87 ppm (t, $^3J=6.7$ Hz, 9H); ^{13}C NMR ($CDCl_3$, 75 MHz): $\delta=166.2$, 153.1, 141.6, 140.6, 128.3, 122.1 (CH), 120.3 (CH), 106.4 (CH), 73.6 (CH_2), 69.6 (CH_2), 57.9 (CH_3), 31.9 (CH_2), 30.4 (CH_2), 29.8 (CH_2), 29.7 (CH_2), 29.5 (CH_2), 29.4 (CH_2), 29.3 (CH_2), 26.2 (CH_2), 26.1 (CH_2), 22.7 (CH_2), 14.1 ppm (CH_3); IR (KBr): $\tilde{\nu}=3393$ (br m), 3293 (br m), 2916 (s), 2848 (s), 1648 (s), 1581 (m), 1468 (s), 1341 (m), 1275 (s), 1123 cm^{-1} (s);

FABMS *m/z* (%): 976.0 (100) $[M-I]^+$; elemental analysis calcd (%) for $C_{64}H_{115}IN_2O_4$: C 69.66, H 10.50, N 2.54; found: C 69.41, H 10.19, N 2.09.

BF_4–C_{14}ammonium: C_{14}ammonium compound with iodine as counterion (201.3 mg) was dissolved in ethanol (50 mL) and $AgBF_4$ (1.1 equiv) was added to the solution to precipitate AgI. The solution was stirred for 4 h to complete the exchange. The AgI precipitate was removed by means of filtration and the solvent evaporated. The C_{14}ammonium compound with BF_4^- as the counterion was recrystallized from a mixture of CH_2Cl_2/CH_3CN by means of slow evaporation of dichloromethane. The effectiveness of the exchange was confirmed by means of elemental analysis: elemental analysis calcd (%) for $C_{58}H_{103}BF_4N_2O_4$: C 71.14, H 10.60, N 2.86; found: C 70.86, H 10.40, N 2.58.

General procedure for the preparation of the adduct (complex): The sulfonate salt (1 equiv) was dissolved in DMF and $C_n$ammonium (1 equiv per negative charge) was added. The mixture was stirred at RT for one day. Water was then added, the precipitate was washed with water, and dried under vacuum. Recrystallization in a mixture of CH_2Cl_2/CH_3CN gave the complexes as powders.

Sulfobodipy–C_{12}ammonium: Yield: 75%; ^{1}H NMR ($CDCl_3$, 200 MHz): $\delta=9.86$ (brs, 2H), 7.63 (br AB, $J_{A,B}=7.7$ Hz, $\nu_0=64.2$ Hz, 8H), 7.33 (s, 4H), 4.06–3.96 (m, 12H), 3.47 (brs, 18H), 2.65–2.56 (m, 12H), 2.01 (brs, 3H), 1.72 (brs, 12H), 1.24 (brs, 108H), 0.86 ppm (brs, 18H); IR (KBr): $\tilde{\nu}=3400$ (brm), 2920 (s), 2916 (s), 2851 (m), 1659 (brm), 1582 (m), 1537 (s), 1497 (s), 1334 (s), 1199 (s), 1114 cm^{-1} (s); UV/Vis (CH_2Cl_2): λ (ε)= 510 (39500), 360 (4400), 284 (36000), 229 nm (35000 $M^{-1}cm^{-1}$); elemental analysis calcd (%) for $C_{118}H_{199}BF_2N_6O_{14}S_2$: C 69.51, H 9.84, N 4.12; found: C 69.92, H 9.99, N 4.37.

Sulfobodipy–C_{14}ammonium: Yield: 82%; ^{1}H NMR ($CDCl_3$, 200 MHz): $\delta=9.83$ (brs, 2H), 7.78 (brs, 4H), 7.48 (brs, 4H), 7.33 (s, 4H), 4.06–3.97 (m, 12H), 3.50 (brs, 18H), 2.64–2.60 (m, 12H), 1.90 (brs, 3H), 1.73 (brs, 12H), 1.24 (brs, 132H), 0.87 ppm (brs, 18H); IR (KBr): $\tilde{\nu}=3398$ (brm), 3270 (brm), 2917 (s), 2849 (s), 1652 (brm), 1582 (m), 1538 (m), 1467 (s), 1335 (s), 1193 (s), 1117 cm^{-1} (s); UV/Vis (CH_2Cl_2): λ (ε)=509 (35500), 362 (4200), 285 nm (3400 $M^{-1}cm^{-1}$); elemental analysis calcd (%) for $C_{130}H_{223}BF_2N_6O_{14}S_2$: C 70.74, H 10.18, N 3.81; found: C 71.14, H 10.42, N 4.12.

Sulfobodipy–C_{16}ammonium: Yield: 72%; ^{1}H NMR ($CDCl_3$, 300 MHz): $\delta=9.84$ (brs, 2H), 7.77 (brs, 4H), 7.43 (brs, 4H), 7.33 (s, 4H), 4.06–3.97 (m, 12H), 3.46 (brs, 18H), 2.62 (brs, 12H), 1.90–1.72 (m, 15H), 1.24 (brs, 156H), 0.87 ppm (brs, 18H); IR (KBr): $\tilde{\nu}=3398$ (brm), 3270 (brm), 2915 (s), 2848 (s), 1645 (brm), 1583 (m), 1538 (m), 1469 (s), 1337 (s), 1191 (s), 1120 cm^{-1} (s); UV/Vis (CH_2Cl_2): λ (ε)=510 (32500), 360 (4500), 285 (24000), 229 nm (23000 $M^{-1}cm^{-1}$); elemental analysis calcd (%) for $C_{142}H_{247}BF_2N_6O_{14}S_2$: C 71.80, H 10.48, N 3.54; found: C 72.14, H 10.67, N 3.84.

TPPS–C_8ammonium: Yield: 42%; ^{1}H NMR ($(CD_3)_2CO$, 300 MHz): $\delta=$ 10.38 (s, 4H), 8.82 (s, 8H), 7.85 (AB, $J_{A,B}=7.3$ Hz, $\nu_0=26.3$ Hz, 16H), 7.96 (s, 16H), 7.21 (s, 8H), 3.96–3.86 (m, 24H), 3.60 (s, 36H), 1.70–1.61 (m, 24H), 1.24 (brs, 120H), 0.85 ppm (brs, 36H); IR (KBr): $\tilde{\nu}=3401$ (brm), 3312 (brm), 2919 (s), 2848 (s), 1655 (s), 1582 (m), 1495 (s), 1468 (s), 1333 (s), 1202 (s), 1185 (s), 1113 (s), 1033 cm^{-1} (s); UV/Vis (CH_2Cl_2): λ (ε)=648 (2500), 592 (3150), 552 (5300), 516 (10800), 418 (300000), 400 (112000), 285 nm (106300 $M^{-1}cm^{-1}$); elemental analysis calcd (%) for $C_{204}H_{294}N_{12}O_{28}S_4$: C 70.19, H 8.49, N 4.81; found: C 70.49, H 8.79, N 4.90.

TPPS–C_{12}ammonium: Yield: 25%; ^{1}H NMR ([D_6]DMSO, 300 MHz): $\delta=$ 10.38 (s, 4H), 8.87 (s, 8H), 8.01 (AB, $J_{A,B}=8.1$ Hz, $\nu_0=38.4$ Hz, 16H), 7.99 (s, 16H), 7.26 (s, 8H), 4.03 (t, $^3J=5.9$ Hz, 18H), 3.92 (t, $^3J=6.5$ Hz, 6H), 3.63 (s, 36H), 1.74–1.64 (m, 24H), 1.27 (brs, 216H), 0.87 ppm (t, 36H, $^3J=6.0$ Hz); IR (KBr): $\tilde{\nu}=3419$ (brm), 3308 (brm), 2919 (s), 2851 (s), 1656 (s), 1581 (m), 1495 (m), 1424 (m), 1332 (s), 1190 (s), 1114 cm^{-1} (s); UV/Vis (CH_2Cl_2) λ (ε)=648 (3200), 592 (4000), 552 (6600), 517 (12600), 418 (360000), 285 nm (110000 $M^{-1}cm^{-1}$); elemental analysis calcd (%) for $C_{252}H_{390}N_{12}O_{28}S_4$: C 72.69, H 9.44, N 4.04; found: C 72.41, H 9.13, N 3.82.

Acknowledgements

This work was jointly supported by Louis Pasteur University through the European School of Polymer and Materials Chemistry (ECPM) and by the Centre National de la Recherche Scientifique (CNRS) of France. We are also indebted to Professor Jack Harrowfield (ISIS Strasbourg) for careful reading and commenting on this manuscript prior to journal submission.

[1] M. O'Neill, S. M. Kelly, *Adv. Mater.* **2003**, *15*, 1135–1146.

[2] a) M. P. Aldred, A. J. Eastwood, S. M. Kelly, P. Vlachos, A. E. A. Contoret, S. R. Farrar, B. Mansoor, M. O'Neill, W. C. Tsoi, *Chem. Mater.* **2004**, *16*, 4928–4936; b) M. Kawamoto, H. Mochizuki, T. Ikeda, B. Lee, Y. Shirota, *J. Appl. Phys.* **2003**, *94*, 6442–6446; c) H. Tokuhisa, M. Era, T. Tsutsui, *Appl. Phys. Lett.* **1998**, *72*, 2639–2641; d) H. Mochizuki, T. Hasui, M. Kawamoyo, T. Shiono, T. Ikeda, C. Adachi, Y. Taniguchi, Y. Shirota, *Chem. Commun.* **2000**, 1923–1924; e) S. Furumi, D. Janietz, M. Kidowaki, M. Nakagawa, S. Morino, J. Stumpe, K. Ichimura, *Chem. Mater.* **2001**, *13*, 1434–1437.

[3] a) B. A. Greeg, M. A. Fox, A. J. Bard, *J. Phys. Chem.* **1990**, *94*, 1586–1598; b) A. M. Fox, J. V. Grant, D. Melamed, T. Torimoto, C.-Y. Liu, A. J. Bard, *Chem. Mater.* **1998**, *10*, 1771–1776; c) L. Schmidt-Mende, A. Fechtenkötter, K. Müllen, E. Moons, R. H. Friend, J. D. MacKenzie, *Science* **2001**, *293*, 1119–1122; d) M. Oukachmih, P. Destruel, I. Seguy, G. Ablart, P. Jolinat, S. Archambeau, M. Mabiala, S. Fouet, H. Bock, *Sol. Energy Mater. Sol. Cells* **2005**, *85*, 535–543.

[4] a) A. M. van de Craats, N. Stutzmann, O. Bunk, M. M. Nielsen, M. Watson, K. Müllen, H. D. Chanzy, H. Sirringhaus, R. Friand, *Adv. Mater.* **2003**, *15*, 495–499; b) M. Katsuara, I. Aoyagi, H. Nakajima, T. Mori, T. Kambayashi, M. Ofuji, Y. Takanishi, K. Ishikawa, H. Takezoe, H. Hosono, *Synth. Met.* **2005**, *149*, 219–223.

[5] a) C. Tschierske, *J. Mater. Chem.* **1998**, *8*, 1485–1508; b) H.-T. Nguyen, C. Destrade, J. Malthête, *Adv. Mater.* **1997**, *9*, 375–388; c) S. Chandrasekhar, B. K. Sadashiva, K. A. Suresh, *Pramana* **1977**, *9*, 471–480; d) G. Gray, J. W. Goodby, *Smectic Liquid Crystals*, Leonard Hill, London, **1984**; e) P. Davidson, J.-C. P. Gabriel, *Curr. Opin. Colloid Interface Sci.* **2005**, *9*, 377–383; f) M. B. Ros, J. L. Serrano, M. R. de la Fuente, C. L. Folcia, *J. Mater. Chem.* **2005**, *15*, 5093–5098; g) J. Barberá, B. Donnio, L. Gehringer, D. Guillon, M. Marcos, A. Omenat, J. L. Serrano, *J. Mater. Chem.* **2005**, *15*, 4093–4105; h) J. L. Serrano, *Metallomesogens*, VCH, Weinheim, **1996**.

[6] a) D. Adam, P. Schuhmacher, J. Simmerer, L. Häussling, K. Siemensmeyer, K. H. Etzbachi, H. Ringsdorf, D. Haarer, *Nature* **1994**, *371*, 141–143; b) A. M. van de Craats, J. M. Warman, A. Fechtenkötter, J. D. Brand, M. A. Harbison, K. Müllen, *Adv. Mater.* **1999**, *11*, 1469–1472; c) M. Lehmann, G. Kestemont, R. G. Aspe, C. Buess-Herman, M. H. J. Koch, M. G. Debije, J. Piris, M. P. de Haas, J. M. Warman, M. D. Watson, V. Lemaur, J. Cornil, Y. H. Geerts, R. Gearba, D. I. Ivanov, *Chem. Eur. J.* **2005**, *11*, 3349–3362; d) N. Boden, R. J. Bushby, J. Clements, B. Movaghar, *J. Mater. Chem.* **1999**, *9*, 2081–2086; e) V. Lemaur, D. A. da Silva Filho, V. Coropceanu, M. Lehmann, Y. Geerts, J. Piris, M. G. Debije, A. M. van de Craats, K. Senthilkumar, L. D. A. Siebbeles, J. M. Warman, J.-L. Brédas, J. Cornil, *J. Am. Chem. Soc.* **2004**, *126*, 3271–3279.

[7] a) K. Kishikawa, S. Furusawa, T. Yamaki, S. Kohmoto, M. Yamamoto, K. Yamaguchi, *J. Am. Chem. Soc.* **2002**, *124*, 1597–1605; b) F. Morale, R. W. Date, D. Guillon, D. W. Bruce, R. L. Finn, C. Wilson, A. J. Blake, M. Schröder, B. Donnio, *Chem. Eur. J.* **2003**, *9*, 2484–2501; c) R. Ziessel, G. Pickaert, F. Camerel, B. Donnio, D. Guillon, M. Cesario, T. Prange, *J. Am. Chem. Soc.* **2004**, *126*, 12403–12413; d) F. Camerel, R. Ziessel, B. Donnio, D. Guillon, *New J. Chem.* **2006**, *30*, 135–139.

[8] a) C. F. J. Faul, M. Antonietti, *Chem. Eur. J.* **2002**, *8*, 2764–2768; b) C. F. J. Faul, M. Antonietti, *Adv. Mater.* **2003**, *15*, 673–683.

[9] F. Camerel, C. F. J. Faul, *Chem. Commun.* **2003**, 1958–1959.

[10] a) Y. Guan, M. Antonietti, C. F. J. Faul, *Langmuir* **2002**, *18*, 5939–5945; b) J. Kadam, C. F. J. Faul, U. Scherf, *Chem. Mater.* **2004**, *16*, 3867–3871.

[11] C. F. J. Faul, M. Antonietti, *Chem. Eur. J.* **2002**, *8*, 2764–2768.
[12] R. Martín-Rapún, M. Marcos, A. Omenat, J. Barberá, P. Romero, J. L. Serrano, *J. Am. Chem. Soc.* **2005**, *127*, 7397–7403.
[13] Z. Wei, T. Laitinen, B. Smarsly, O. Ikkala, C. F. J. Faul, *Angew. Chem.* **2005**, *117*, 761–766; *Angew. Chem. Int. Ed.* **2005**, *44*, 751–756 .
[14] a) F. Camerel, M. Antonietti, C. F. J. Faul, *Chem. Eur. J.* **2003**, *9*, 2160–2166; b) T. Zhang, C. Spitz, M. Antonietti, C. F. J. Faul, *Chem. Eur. J.* **2005**, *11*, 1001–1009; c) A. Taguchi, T. Abe, M. Iwamoto, *Adv. Mater.* **1998**, *10*, 667–669; d) S. Polarz, B. Smarsly, M. Antonietti, *Chem. Phys. Chem.* **2001**, *7*, 457–461; e) D. G. Kurth, P. Lehmann, D. Volkmer, H. Cölfen, M. J. Koop, A. Müller, A. Du Chesne, *Chem. Eur. J.* **2000**, *6*, 385–393; f) D. Volkmer, A. Du Chesne, D. G. Kurth, H. Schnablegger, P. Lehmann, M. J. Koop, M. A. Müller, *J. Am. Chem. Soc.* **2000**, *122*, 1995–1998.
[15] a) Y. Guan, Y. Zakrevskyy, J. Stumpe, M. Antonietti, C. F. J. Faul, *Chem. Commun.* **2003**, 894–895; b) Y. Zakrevskyy, C. F. J. Faul, Y. Guan, J. Stumpe, *Adv. Funct. Mater.* **2004**, *14*, 835–841.
[16] F. Camerel, P. Strauch, M. Antonietti, C. F. J. Faul, *Chem. Eur. J.* **2003**, *9*, 3764–3771.
[17] a) D. Franke, M. Vos, M. Antonietti, N. A. J. M. Sommerdijk, C. F. J. Faul, *Chem. Mater.* **2006**, *18*, 1839–1847; b) D. Ganeva, M. Antonietti, C. F. J. Faul, R. Sanderson, *Langmuir* **2003**, *19*, 6561–6565; c) A. G. Cook, U. Baumeister, C. Tschierske, *J. Mater. Chem.* **2005**, *15*, 1708–1721; d) W. Li, W. Bu, H. Li, L. Wu, M. Li, *Chem. Commun.* **2005**, 3785–3787; e) M. Marcos, R. Martín-Rapún, A. Omenat, J. Barberá, J. L. Serrano, *Chem. Mater.* **2006**, *18*, 1206–1212; f) J. H. Carmeron, A. Facher, G. Lattermann, S. Diele, *Adv. Mater.* **1997**, *9*, 398–403; g) D. Franke, C. C. Egger, B. Smarsly, C. F. J. Faul, G. J. T. Tiddy, *Langmuir* **2005**, *21*, 2704–2712.
[18] X. Zhu, B. Tartsch, U. Beginn, M. Möller, *Chem. Eur. J.* **2004**, *10*, 3871–3878.
[19] a) H. Eichhorn, *J. Porphyrins Phthalocyanines* **2000**, *4*, 88–102; b) J. Simon, J.-J. André, *Molecular Semiconductors,* Springer, Berlin, **1985**.
[20] F. Camerel, L. Bonardi, M. Schmutz, R. Ziessel, *J. Am. Chem. Soc.* **2006**, *128*, 4548–4549.
[21] F. Camerel, G. Ulrich, R. Ziessel, *Org. Lett.* **2004**, *6*, 4171–4174, and references therein.
[22] J. H. Boyer, A. M. Haag, G. Sathyamoorthi, M.-L. Soong, K. Thangaraj, T. G. Pavlopoulos, *Heteroat. Chem.* **1993**, *4*, 39–49.
[23] J. Karolin, L. B.-A. Johansson, L. Strandberg, T. Ny, *J. Am. Chem. Soc.* **1994**, *116*, 7801–7806.
[24] V. N. Knyukshto, K. N. Solovyov, G. D. Egorova, *Biospectroscopy* **1998**, *4*, 121–133.
[25] J. Olmsted, *J. Phys. Chem.* **1979**, *83*, 2581–2584.
[26] a) V. Paganuzzi, P. Guatteri, P. Riccardi, T. Sacchelli, J. Barberá, M. Costa, E. Dalcanale, *Eur. J. Org. Chem.* **1999**, 1527–1539; b) M. Castella, F. Lopez-Calhorra, D. Velasco, H. Finkelmann, *Chem. Commun.* **2002**, 2348–2349; c) B. A. Gregg, M. A. Fox, A. J. Bard, *J. Am. Chem. Soc.* **1989**, *111*, 3024–3029.
[27] a) R. G. Snyder, S. L. Hsu, S. Krimm, *Spectrochim. Acta, Part A* **1978**, *34*, 395–406; b) X. Du, B. Shi, Y. Liang, *Spectrosc. Lett.* **1999**, *32*, 1–16; c) N. Yamada, T. Imai, E. Koyama, *Langmuir* **2001**, *17*, 961–963.
[28] a) T. Kato, T. Kutsuna, K. Hanabusa, M. Ukon, *Adv. Mater.* **1998**, *10*, 606–608; b) K. Hanabusa, C. Koto, M. Kimura, H. Shirai, A. Kakehi, *Chem. Lett.* **1997**, 429–430.
[29] R. M. Silverstein, G. C. Bassler, T. C. Morrill, *Spectrometric Identification of Organic compounds*, 3rd ed., Wiley, New York, **1976**.
[30] a) F. Morale, R. W. Date, D. Guillon, D. W. Bruce, R. L. Finn, C. Wilson, A. J. Blake, M. Schröder, B. Donnio, *Chem. Eur. J.* **2003**, *9*, 2484–2501; b) B. Donnio, B. Heinrich, H. Allouchi, J. Kain, S. Diele, D. Guillon and D. W. Bruce, *J. Am. Chem. Soc.* **2004**, *126*, 15258–15268.
[31] D. Guillon, *Struct. Bonding (Berlin)* **1999**, *95*, 41–82.
[32] M. Benouazzane, S. Coco, P. Espinet, J. Barberá, *J. Mater. Chem.* **2001**, *11*, 1740–1744.
[33] T. Yasuda, K. Kishimoto, T. Kato, *Chem. Commun.* **2006**, 3399–3401.
[34] T. Hatano, M. Takeuchi, A. Ikeda, S. Shinkai, *Org. Lett.* **2003**, *5*, 1395–1398.
[35] M. Kimura, H. Ueki, K. Ohta, K. Hanabusa, H. Shirai, N. Kobayashi, *Chem. Eur. J.* **2004**, *10*, 4954–4959.

Received: October 18, 2006
Published online: January 24, 2007

